

Article

# The Impact of Offshore Photovoltaic Utilization on Resources and Environment Using Spatial Information Technology

Peng Wang <sup>1</sup>, Jingru Zhou <sup>2</sup>, Xinfei Jin <sup>3</sup>, Jingchao Shi <sup>4</sup>, Ngai Weng Chan <sup>5</sup> , Mou Leong Tan <sup>5</sup> , Xingwen Lin <sup>2</sup> , Xu Ma <sup>6</sup> , Xia Lin <sup>7</sup>, Kaixuan Zheng <sup>1,8</sup>, Jiexuan Wu <sup>1,8</sup> and Fei Zhang <sup>2,\*</sup> 

<sup>1</sup> Marine Academy of Zhejiang Province, Hangzhou 310012, China; wangpeng19860223@126.com (P.W.); hkyzhengkx@163.com (K.Z.); wujiexuan129@163.com (J.W.)

<sup>2</sup> College of Geography and Environmental Sciences, Zhejiang Normal University, Jinhua 321004, China; 18755737941@163.com (J.Z.); linxw@zjnu.edu.cn (X.L.)

<sup>3</sup> Shengyong Marine Technology Limited Company of Ningbo, Ningbo 315042, China; jxf0506@163.com

<sup>4</sup> Department of Earth Sciences, The University of Memphis, Memphis, TN 38152, USA; jshi@memphis.edu

<sup>5</sup> GeoInformatic Unit, Geography Section, School of Humanities, Universiti Sains Malaysia, Gelugor 11800, Malaysia; nwchan@usm.my (N.W.C.); mouleong@usm.my (M.L.T.)

<sup>6</sup> College of Geography and Remote Sensing Sciences, Xinjiang University, Urumqi 830017, China; maxu2020@xju.edu.cn

<sup>7</sup> National Marine Environmental Monitoring Center, Dalian 116023, China; linxia@nmemc.gov.cn

<sup>8</sup> Key Laboratory of Ocean Space Resource Management Technology, Hangzhou 310012, China

\* Correspondence: zhangfei3s@163.com or zhangfei3s@zjnu.edu.cn

**Abstract:** In recent years, the rapid development of the photovoltaic (PV) industry has resulted in a saturation of research on onshore PV power plant construction. However, current studies on the impact of marine PVs on the marine environment remain limited and scarce. In order to facilitate the implementation of carbon reduction goals and promote the sustainable development of the offshore PV industry, this study analyzes the environmental impact of PV sea-use resources based on spatial information technology in the western part of Gaotang Island. The findings show that the MIKE21FM model provides relatively accurate simulations of tidal flow and tide level in the marine PV area. Flow velocity in the marine PV area exhibits a decreasing trend, with an average decrease ranging from 0.03 to 0.07 m/s. This decrease minimally affects surrounding navigational channels and large-scale flow fields. The resulting siltation is also deemed less significant, with an annual deposition from 0.03 to 0.06 m/a. Moreover, offshore PV construction resulted in a total intertidal biological loss of 123.45 t. The suspension of sediment during cofferdam construction and removal has a potential effect on zooplankton and fishery resources. Overall, it is proposed that careful planning, prudent site selection, and the execution of countermeasures during marine PV construction will combine to minimize the impact on the marine environment.

**Keywords:** PV; energy; marine environment; RS; GIS; solar



**Citation:** Wang, P.; Zhou, J.; Jin, X.; Shi, J.; Chan, N.W.; Tan, M.L.; Lin, X.; Ma, X.; Lin, X.; Zheng, K.; et al. The Impact of Offshore Photovoltaic Utilization on Resources and Environment Using Spatial Information Technology. *J. Mar. Sci. Eng.* **2024**, *12*, 837. <https://doi.org/10.3390/jmse12050837>

Academic Editor: Atilla Incecik

Received: 6 April 2024

Revised: 9 May 2024

Accepted: 15 May 2024

Published: 17 May 2024



**Copyright:** © 2024 by the authors. Licensee MDPI, Basel, Switzerland. This article is an open access article distributed under the terms and conditions of the Creative Commons Attribution (CC BY) license (<https://creativecommons.org/licenses/by/4.0/>).

## 1. Introduction

Solar energy, as a clean and renewable power source, is one of the most ideal alternatives to traditional energy sources, such as oil, natural gas, and coal [1]. The principle of PV power generation is to convert solar radiation resources into electricity based on the “PV effect”, which is a new type of solar energy utilization [2]. Currently, the global installed capacity of PV power generation has exceeded 1000 GW, accounting for approximately 1% of the global installed capacity of power generation [3]. PV power generation is of strategic importance in accelerating the formation of a new pattern of clean electricity utilization and achieving the dual carbon goals [4]. The Chinese government always attached great importance to the development and utilization of new and renewable energy sources, actively promoting their development and improving the electricity structure [5]. The construction of offshore PV power plants is in line with the requirement of “developing clean energy and

practicing a green and low-carbon strategy”, which is conducive to promoting the transformation and upgrading of the PV power generation industry, advancing “PV+” applications, and achieving win-win results in PV agriculture. With the rapid development of renewable electricity in China, including PV power generation, new energy sources are becoming the main force to optimize the energy structure and achieve the “dual carbon” goals. In recent years, many scholars have conducted research on the ecological and environmental impacts of terrestrial PVs. PV modules in PV power plants can change the proportion of diffused radiation and direct radiation, which can affect the photosynthetic rate of plants [6]. Therefore, a decrease in the photosynthetically active radiation may lead to a reduction in the photosynthetic rate of plants under PV modules [7]. Some researchers also found that terrestrial PV modules may lower soil temperature [8], increase soil moisture content [9], and induce changes in soil physical and chemical environments [10]. However, there is limited research on the impact of marine PVs on the marine environment. Due to the high population density and limited per capita land area in China, the development of land-based PV power plants is increasingly restricted [11]. Therefore, the development of offshore PVs is increasingly seen as the way forward [12–15].

According to the data from the National Energy Administration, China’s cumulative installed capacity of renewable electricity power generation has reached 1.213 billion kilowatts as of the end of 2022, which represents a 14.1% increase compared to 2021, accounting for 47.3% of the total installed capacity of electricity, with PV power generation reaching 427.3 billion kilowatts (<https://finance.sina.com.cn/jjxw/2023-09-19/doc-imznfexh8870291.shtml>) (accessed on 15 March 2024). The PV industry has achieved rapid development, with a growth rate higher than that of other renewable energy sources such as wind power and biomass. Since the “13th Five-Year Plan,” Zhejiang Province attached great importance to the development of renewable power and achieved significant results. The “14th Five-Year Plan for Energy Development in Zhejiang Province” ([https://www.zj.gov.cn/art/2022/5/19/art\\_1229019365\\_2404305.html](https://www.zj.gov.cn/art/2022/5/19/art_1229019365_2404305.html)) (accessed on 15 March 2024) and the “14th Five-Year Plan for the Development of Renewable Energy in Zhejiang Province” (<https://huanbao.bjx.com.cn/news/20210623/1159909.shtml>) (accessed on 15 March 2024) proposed the implementation of the “Wind and Solar Power Doubles” project during the “14th Five-Year Plan” period, aiming to achieve an increase of over 12 million kilowatts in PV-installed capacity, with centralized PV installation exceeding 7 million kilowatts.

Due to the geographical features of the “Seven Mountains, Two Waters, and One Farmland” in Zhejiang Province, there are limited development opportunities for land-based centralized PVs. However, the province has abundant tidal flat resources in its coastal areas possessing huge potential for offshore PV development [16]. The PV industry cluster in Zhejiang Province has distinct characteristics and formed a pattern led by Jiaxing and Jinhua (Yiwu), promoting coordinated development in cities like Hangzhou, Ningbo, Huzhou, and Quzhou. In 2022, the total output value of the new energy industry in Jiaxing exceeded CNY 100 billion, with the PV industry achieving an output value of CNY 81.5 billion, a year-on-year increase of 50%, accounting for one-third of the PV industry’s output value in the province. The Yiwu PV industry achieved a scale output value of CNY 90.2 billion, accounting for over 30% of the PV industry’s output value in Zhejiang Province. As of 2022, there were 184 PV companies in Zhejiang Province, with a total output value of CNY 249.86 billion, a year-on-year increase of 64.9%. The PV module production reached 98 GW, accounting for 33.9% of the national output (<https://www.163.com/dy/article/IH8BQSR205198SOQ.html>) (accessed on 15 March 2024). The installed capacity of PVs in Zhejiang Province reached 25.39 GW in 2022, ranking third nationwide with a year-on-year growth of 37.84%. By the first half of 2023, the installed capacity of PVs in Zhejiang Province is expected to reach 28.56 GW (<https://www.163.com/dy/article/IH6PU9F5051481OF.html>) (accessed on 15 March 2024). Coastal cities in Zhejiang Province are actively planning for the development of offshore PV industries, and both the number of planned projects and the scale of construction are experiencing explosive growth [17]. However, will the construction and development of offshore

PVs have an impact on the marine environment? In view of this question, this study focuses on a research area in the western part of Gaotang Island and analyzes the environmental impact of offshore PV resources using spatial information technology. The specific tasks include: (1) analyzing tidal currents and tide level changes in the offshore PV area and exploring changes in flow patterns and sedimentation in the area, and (2) evaluating the ecological and resource impact of offshore PV development. Our study contributes to understanding the impacts of offshore photovoltaic utilization on environmental resources and ecology. The novelty of this study is the verification of the environmental impact of this new offshore PV energy model. This study anticipates establishing relevant energy facilities under minimal impact conditions.

## 2. Overview of the Study Area

The study area is located in the southern part of Changda Wetland, where the tidal flats are, on the west side of Gaotang Island, Xiangshan County, Ningbo City, southeast of Xiayang Wetland Polder Area, Ninghai County. It is approximately 20 km away from the S19 Expressway, 38 km from Xiangshan County, and 90 km from Ningbo City. The geographical coordinates are approximately  $29.13^{\circ}$  N and  $121.77^{\circ}$  E. The PV area is located in the northern part of Changda Wetland, the tidal flat on the west side of Gaotang Island, Xiangshan County. It is bordered by the Gaotang Changda Wetland Reclamation Project to the east, Baijiao Waterway to the west, and Sanmen Waterway and Yueyingyang to the north. The total installed photovoltaic capacity in the study area is 159.06175 MWp and a land area of approximately 2458 acres. The research area has a relatively flat terrain, with elevations ranging from  $-1.0$  m to  $2.2$  m (85 elevation). It is located in a subtropical monsoon climate zone with maritime characteristics, characterized by mild and humid weather and distinct seasons, with an average temperature of  $17.8^{\circ}$  C. The average annual precipitation ranges from 1322.5 mm to 1390.6 mm, and the average relative humidity ranges from 76% to 86%, as shown in Figure 1.

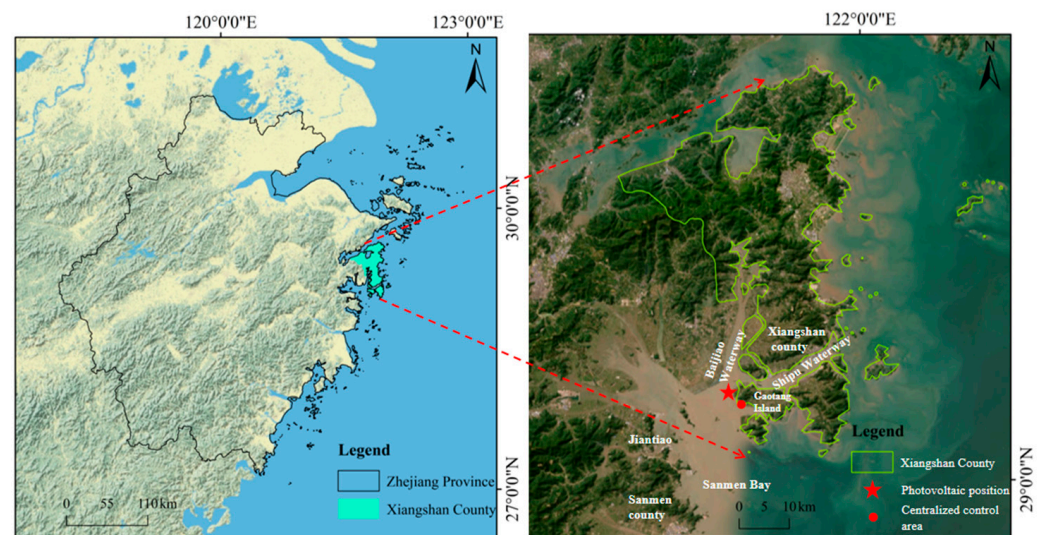


**Figure 1.** Schematic map of the study area.

In this study, the offshore PV is a mudflat power plant, close to the seashore, and in order to consider the subsequent stable operation of the power plant, a wave retaining wall of about 3 km was set up on the outside of the PV power plant. The total length of the temporary cofferdam on the outside of the PV power project in the study area is about 3 km, which is located between the wave barrier wall and the PV array area (Figure 2), and the top of the temporary cofferdam adopts a non-permeable form.

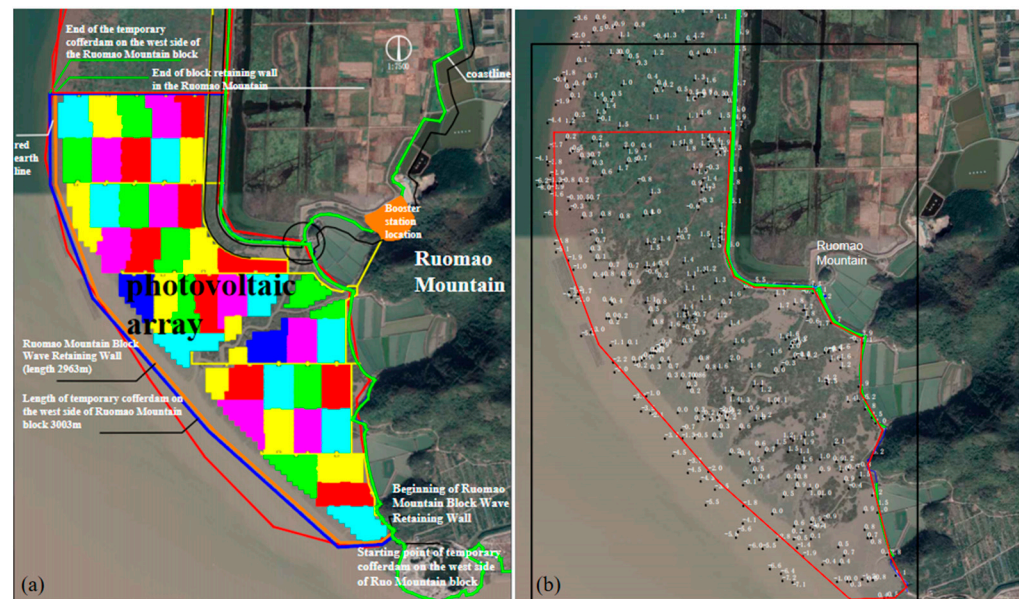


**Figure 2.** PV location map ((a). Marine PV layout (Different colors represent the individual power generation units in the project); (b). Topographic map of the bathymetry of the PV area).

### 3. Data Processing and Research Methods

#### 3.1. Marine Hydrographic Data

##### 3.1.1. Hydrographic Observation Data

Seven hydrological and sediment stations (N01~N07), two temporary tide stations (W1~W2), which are located near the project, were selected for synchronous observations during three tidal cycles: spring tide, neap tide, and mean tide (Figure 3). The duration of continuous observation was not less than 27 h, and the observation period was January 2020. The tide level was measured using a TGR-2050 pressure-type tide gauge, and a vertical staff gauge was used for benchmark comparison. The tidal reference plane was based on the 1985 national elevation datum, and the zero elevation of the staff gauge was determined by fourth-order leveling. Fixed-point current observations were conducted using an SLC9-2 direct-reading current meter. Suspended sediment concentration was measured using a horizontal water sampler or an inverted water sampler, filtration device, and a one-thousandth electronic balance. Suspended sediment was measured using a laser particle size analyzer. Bottom sediment samples were collected using a grab sampler and a laser particle size analyzer. Basic information from the hydrological data observation stations are shown in Table 1.

##### 3.1.2. Marine Ecological Survey Data

The water quality, sediment, ecological environment, and fishery resources survey data in this study are shown in Figure 4. The content of the survey is shown in Table 2.

#### 3.2. Hydrodynamic Research Methods

##### 3.2.1. Mathematical Modeling

A two-dimensional numerical model MIKE21FM [22] developed by the Danish Hydraulic Institute was used to study the hydrodynamic variations in the engineering area. The model uses an unstructured triangular mesh for the computational domain, as this can fit the land boundary well. The grid design is flexible, and the grid density can be controlled arbitrarily. The software (Version 2014) has the advantages of reliable algorithms, stable calculations, a user-friendly interface, and powerful pre- and post-processing capabilities. It has been applied to coastal engineering projects in multiple countries. MIKE21FM uses the standard finite volume method for horizontal spatial discretization and the first-order

explicit Euler difference format for temporal discretization of the momentum equation and transport equation. The model control equations are as follows:

Mass conservation equations:

$$\frac{\partial \zeta}{\partial t} + \frac{\partial}{\partial x}(hu) + \frac{\partial}{\partial y}(hv) = 0 \tag{1}$$

Momentum equation:

$$\frac{\partial u}{\partial t} + u \frac{\partial u}{\partial x} + v \frac{\partial u}{\partial y} - \frac{\partial}{\partial x} \left( \varepsilon_x \frac{\partial u}{\partial x} \right) - \frac{\partial}{\partial y} \left( \varepsilon_x \frac{\partial u}{\partial y} \right) - fv + \frac{gu\sqrt{u^2 + v^2}}{C_z^2 H} = -g \frac{\partial \zeta}{\partial x} - \frac{1}{\rho_0} \frac{\partial p_a}{\partial x} \tag{2}$$

$$\frac{\partial v}{\partial t} + u \frac{\partial v}{\partial x} + v \frac{\partial v}{\partial y} - \frac{\partial}{\partial x} \left( \varepsilon_y \frac{\partial v}{\partial x} \right) - \frac{\partial}{\partial y} \left( \varepsilon_y \frac{\partial v}{\partial y} \right) + fu + \frac{gv\sqrt{u^2 + v^2}}{C_z^2 H} = -g \frac{\partial \zeta}{\partial y} - \frac{1}{\rho_0} \frac{\partial p_a}{\partial y} \tag{3}$$

where  $\zeta$  is the water level;  $h$  is the static water depth;  $H$  is the total water depth;  $H = h + \zeta$ ;  $u$  and  $v$  are the vertical mean flow velocity in the  $x$  and  $y$  directions, respectively;  $g$  is the gravitational acceleration,  $g = 9.81 \text{ m/s}^2$ ;  $f$  is the Kurtosis force parameter ( $f = 2\omega \sin\varphi$ ,  $\varphi$  is the geographic latitude where the calculated sea area is located);  $C_z$  is the Chezy coefficient (it is an important parameter in the MIKE21FM model to characterize the frictional resistance of the seabed, i.e., the frictional resistance of seawater flowing through the seabed),  $C_z = \frac{1}{n} H^{\frac{1}{6}}$ ,  $\varepsilon_x$  and  $\varepsilon_y$  are the horizontal vortex viscous coefficients in the  $x$  and  $y$  directions, respectively,  $n$  is the Manning coefficient,  $\rho_0$  is the density of water, and  $p_a$  is the atmospheric pressure.

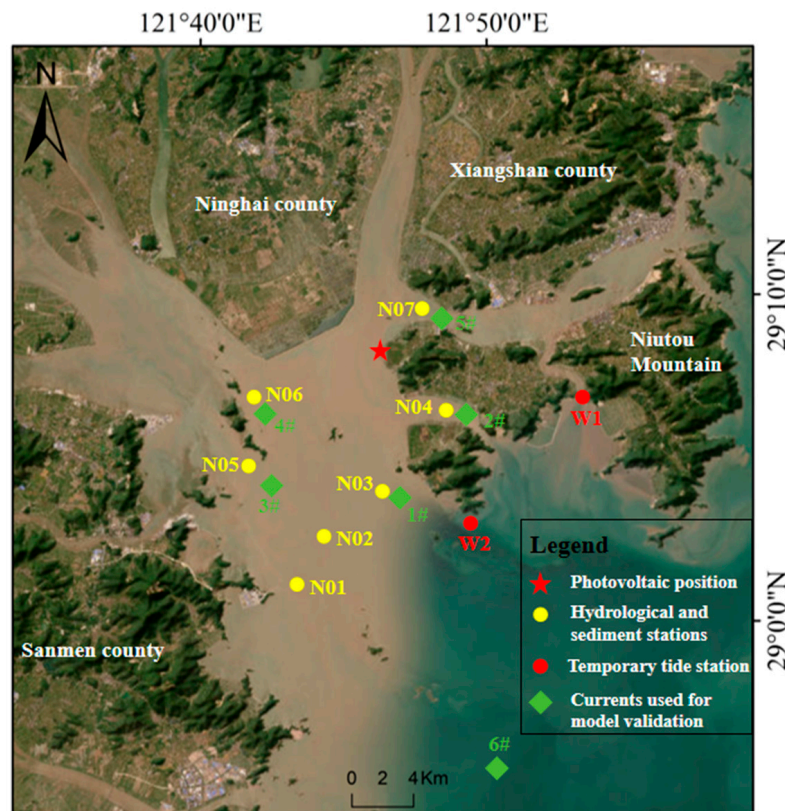


Figure 3. Distribution map of hydrological and sediment observation stations.

The initial conditions for the solution of the equations are shown in Equation (4), and the boundary conditions are shown in Equation (5). The solid boundary takes the normal

flow velocity as zero, and the dynamic boundary is used in the tidal flat area; the water boundary is controlled by the forecast tide level.

$$\begin{cases} \zeta(x, y, t)|_{t=t_0} = \zeta(x, y, t_0) = 0 \\ u(x, y, t)|_{t=t_0} = v(x, y, t)|_{t=t_0} = 0 \end{cases} \quad (4)$$

$$\vec{V} \cdot \vec{n} = 0 \quad (5)$$

The flowchart of this paper is shown in Figure 5.

Table 1. Basic information from hydrological data observation stations.

Observation Station	Bathymetry (m)	Test Content
N01	7.2	Fixed-point flow measurement, sand content, suspended sand, substrate quality
N02	7.3	Fixed-point flow measurement, sand content, suspended sand, substrate quality
N03	5.8	Fixed-point flow measurement, sand content, suspended sand, substrate quality
N04	14.4	Fixed-point flow measurement, sand content, suspended sand, substrate quality
N05	8.5	Fixed-point flow measurement, sand content, suspended sand, substrate quality
N06	12.6	Fixed-point flow measurement, sand content, suspended sand, substrate quality
N07	21.5	Fixed-point flow measurement, sand content, suspended sand, substrate quality
W1		Tide level
W2		Tide level

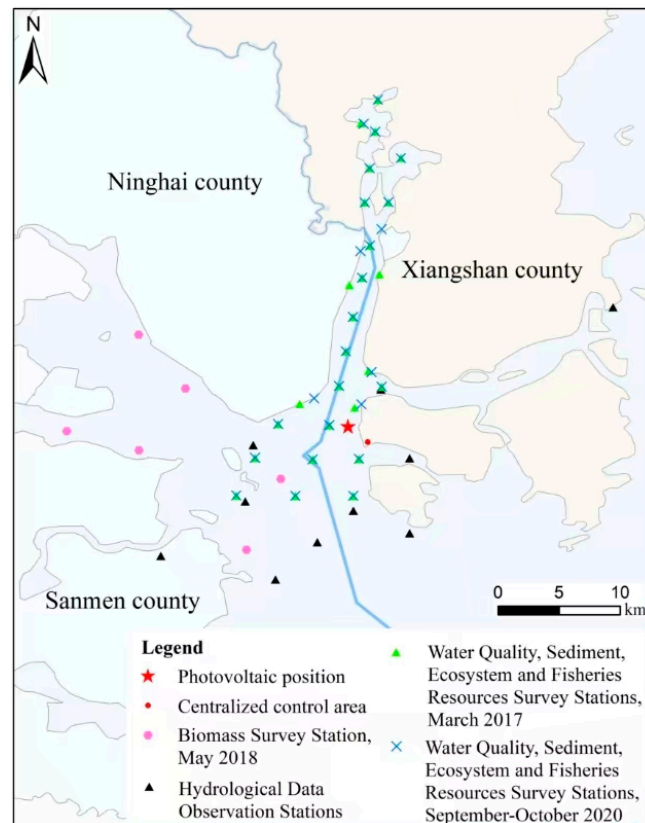
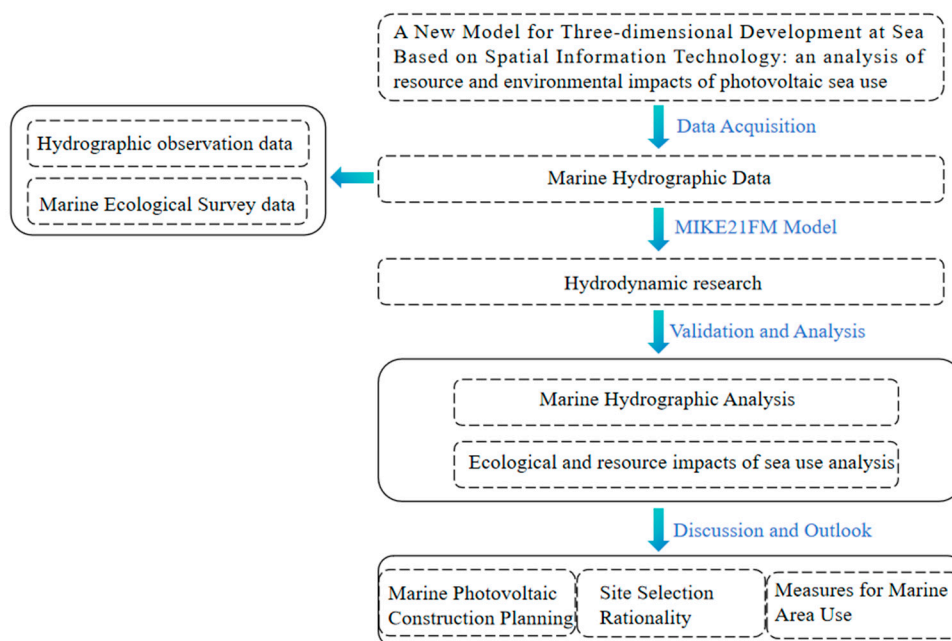


Figure 4. Map of survey stations for marine ecological survey data.

**Table 2.** Content of marine ecological surveys.

Investigative Projects	Survey Methods
Water samples	Surface water samples were collected from water depths less than 10 m, while surface and bottom water samples were collected from depths greater than 10 m. Petroleum samples were collected only at the surface.
Plankton	Phytoplankton: Nets were used, and a shallow water type III vertical trawl net was used for shallow water areas. Zooplankton: Nets were used (shallow water type I net).
Benthic organisms	a. Survey method in 2017: Bottom sediment was collected using a 0.05 m <sup>2</sup> mud bucket, with two collections made at each station, and the average value of the two collections was taken as the biomass and population density of the station. b. Survey method in 2020: A sediment sampler (0.1 m <sup>2</sup> ) was used for collection, with four collections made at each station, and the average value of the four collections was taken as the biomass and population density of the station.
Intertidal zone organisms	a. Survey method in 2017: Sampling frames of 0.5 m × 0.5 m were used in the high, middle, and low intertidal zones. After filtration through sieves with aperture sizes of 5.0, 1.0, and 0.5 mm, the species composition, biomass, and population density were recorded. Qualitative and quantitative samples were also collected on foot and fixed with formalin for laboratory analysis and identification. b. Survey method in 2020: For each cross-section of the intertidal zone, four quantitative sampling points were set for the high, middle, and low intertidal zones, with a randomly selected sampling area of 0.0625 m <sup>2</sup> and a depth of 30 cm. The organisms were collected through a 1 mm <sup>2</sup> aperture sieve, and qualitative specimens were collected around each sampling point, with substrate conditions recorded.
Biomass	Representative local organisms were selected from the biological samples collected from the 12 large-area stations during autumn fisheries resource trawling in September 2020 for biomass analysis. The sample collection, storage, pretreatment, and analysis were conducted according to the standard methods in the “Marine Survey Specifications” (GB12763-2007) [18]. Fish and crustaceans collected during the May 2018 swimming organism survey, and shellfish collected during the intertidal zone survey were also subjected to biomass analysis.
Fishery resources survey	Fish eggs and larvae surveys were conducted simultaneously with the marine ecological survey, with survey stations matching those of the marine ecological survey. The methods for fish eggs and larvae surveys were carried out in accordance with the “Marine Monitoring Specifications” (GB17378.7-2007) [19]. Swimming organism fixed-point trawl surveys were conducted according to the “Marine Fishery Resources Survey Specifications” (SC/9403-2012) [20] and the “Technical Regulations for Environmental Impact Assessment of Construction Projects on Marine Biological Resources” (SC/T9110-2007) [21].



**Figure 5.** Flowchart of this study.

### 3.2.2. Model Setting

In the MIKE21FM model, the PV pile foundations were set in the model run as five meters of land above the 85 National Elevation and the grid was a dry grid with the same shape, size, and arrangement as the construction design.

- Model calculation area:

The calculation area of the model should be large enough to include the sea area that can be affected by the marine PV area.

- Calculation domain mesh segmentation:

The non-structural triangular mesh is used to dissect the computational domain, and the mesh sparsity and scale are controlled by the mesh generation module. The mesh is encrypted in the sea area near the project area, and the mesh scale is at least 5 m, which can portray the shoreline characteristics well and ensure sufficient computational accuracy. In the sea area far away from the project, the grid is relatively sparse; the grid scale is 1500~9000 m; and the smooth transition between different scale grids is realized through the settings.

- Model shoreline and underwater topography:

The accuracy of underwater terrain data has an extremely important effect on the model calculation. The large-scale underwater topography in the computational domain is digitized from the charts of the Naval Navigation and Protection Department through GIS, and the latest CAD data of underwater topography is used in the sea area near the project. All the databases are unified to the mean sea level.

- Boundary conditions:

The open boundary reconciliation constants are obtained from the OTIS East China Sea ocean model, and then the water level forecast is made for the open boundary according to the obtained reconciliation constants. The forecast formula is as in Equation (6):

$$\zeta = A_0 + \sum_{i=1}^{11} H_i F_i \cos[\sigma_i t - (v_0 + u)_i + g_i] \quad (6)$$

where  $A_0$  is the mean sea surface;  $F_i$  and  $(v_0 + u)_i$  are astronomical elements;  $\sigma_i$  is the angular frequency; and  $H_i$  and  $g_i$  are the tuning constants; i.e., amplitude and latitude angle of a certain subtide, 11 subtides (M2, S2, N2, K2, K1, O1, P1, Q1, M4, MS4, M6) are used for the time-by-time tide prediction, and then the water level is interpolated to each open boundary point.

- Calculation time step:

The calculation time step of the model is dynamically adjusted according to the CFL conditions to ensure the model calculation is stable, with an average time step of 0.5 s and the shortest time step of 0.01 s. The modeling time step is 0.5 s and the shortest time step of 0.01 s, respectively.

- Bed roughness coefficient:

Based on the measured hydrological data, the model was calibrated multiple times. Then, we selected the optimal value to minimize the error; the optimal bed roughness coefficient is 0.0125.

- Horizontal eddy viscosity coefficient:

The horizontal vortex viscosity coefficient was calculated using the Smagorinsky (1963) formula that takes into account subscale grid effects, and the expression is given

in Equation (7), where  $c_s$  is a constant, and  $l$  is the characteristic mixing length, which is obtained from the following calculation:  $S_{ij} = \frac{1}{2}(\frac{\partial u_i}{\partial x_j} + \frac{\partial u_j}{\partial x_i})$  ( $i, j = 1, 2$ ).

$$A = c_s^2 l^2 \sqrt{2S_{ij}S_{ij}} \tag{7}$$

- Koch’s force:

The Koch force varies with latitude, and the specific formula is  $f = 2\omega \sin \phi$ , with  $\phi$  being the geographic latitude at which the sea area is calculated, and  $\omega$  is the angular velocity of the Earth’s rotation and is a constant.

### 3.3. Assessment of Damage to Marine Living Resources

#### 3.3.1. Assessment Methodology

This method is applicable to the occupation of fishery waters due to engineering and construction needs, so that the function of fishery waters is destroyed, or the habitat of marine living resources is lost, and the assessment of damage to various types of living resources is calculated according to Formula (8) [23]:

$$W_i = D_i \times S_i \tag{8}$$

where  $W_i$  is the amount of damage to the biological resources of species  $i$ , in units of tails, individuals, and kg;  $D_i$  is the density of the biological resources of species  $i$  in the assessment area, in units of tails/km<sup>2</sup>, tails/km<sup>3</sup>, and kg/km<sup>2</sup>; and  $S_i$  is the area or volume of fishery waters occupied by the biological resources of species  $i$ , in units of km<sup>2</sup> or km<sup>3</sup>.

#### 3.3.2. Assessment of Damage to Marine Living Resources within the Dispersal Range of Pollutants

The construction process generates suspended matter, the spread of which can cause damage to living marine resources, categorized as one-time average damage and cumulative damage. One-time average damage: the area of incremental pollutant concentration that exists for less than 15 days (including 15 days); Cumulative damage: the area of incremental pollutant concentration that exists for more than 15 days (including 15 days).

##### (1) One-time average damage assessment

The damage to marine living resources caused by the incremental increase in the concentration of a pollutant exceeding the standard value of Class II in GB 11607 [24] or GB 3097 [25] (for pollutants not listed in GB 11607 or GB 3097, the labeled value is derived by analogy with the results of toxicity tests) is calculated in accordance with Formula (9) [19]:

$$W_i = \sum_{j=1}^n D_{ij} \times S_j \times K_{ij} \tag{9}$$

where  $W_i$  is the one-time average loss of biological resources of species  $i$  in tails, individuals, and kg;  $D_{ij}$  is the density of biological resources of species  $i$  in the concentration increment area of category  $j$  of a pollutant in tails/km<sup>2</sup>, individuals/km<sup>2</sup> and kg/km<sup>2</sup>;  $S_j$  is the area of the concentration increment area of category  $j$  of a pollutant in km<sup>2</sup>;  $K_{ij}$  is the rate of loss of biological resources of species  $i$  in the concentration increment area of category  $j$  of a pollutant in percent; and  $n$  is the total number of concentration increment subdivisions of a pollutant.

##### (2) Cumulative damage assessment

When an area of incremental pollutant concentration exists for more than 15 days, the cumulative damage to biological resources shall be calculated, and the calculation of the cumulative damage to biological resources in terms of years shall be calculated according to Formula (10) [23]:

$$M_i = W_i \times T \tag{10}$$

where  $M_i$  is the cumulative damage to biological resources of species  $i$ , in units of tails, individuals, and kg;  $W_i$  is the average damage to biological resources of species  $i$  at one time, in units of tails, individuals, and kg; and  $T$  is the number of cycles of incremental impacts of pollutant concentrations (the actual number of days of impacts in a year divided by 15), in units of individuals.

#### 4. Results and Analysis

##### 4.1. Marine Hydrographic Analysis

##### 4.1.1. Tide Level and Current Verification

The tidal oscillation in the sea area near the study area is mainly formed by the co-oscillation caused by Pacific tides. The East China Sea progressive wave system, dominated by the M2 tide, controls the tidal motion in this area. The northwest Pacific tides enter the sea area near Sanmen Bay in Zhejiang Province from the southeast and northwest. Due to the influence of the friction between terrain and bottom, the tides are deformed. The waveforms, wave velocities, and shallow water tides change. In this study, tide level data from two tide stations (W1~W2) were used for analysis. Figure 6 shows the model setup process, and Figure 7 shows the tidal verification plot. The observed tidal levels during spring and neap tides fit well with the simulated tidal levels, with a simulation error generally within 0.4 m. The simulated tidal phases are basically consistent with the observations, with small errors. This demonstrates that the model provides accurate simulations of tidal levels; tidal elevation discrepancies are shown in Table 3.

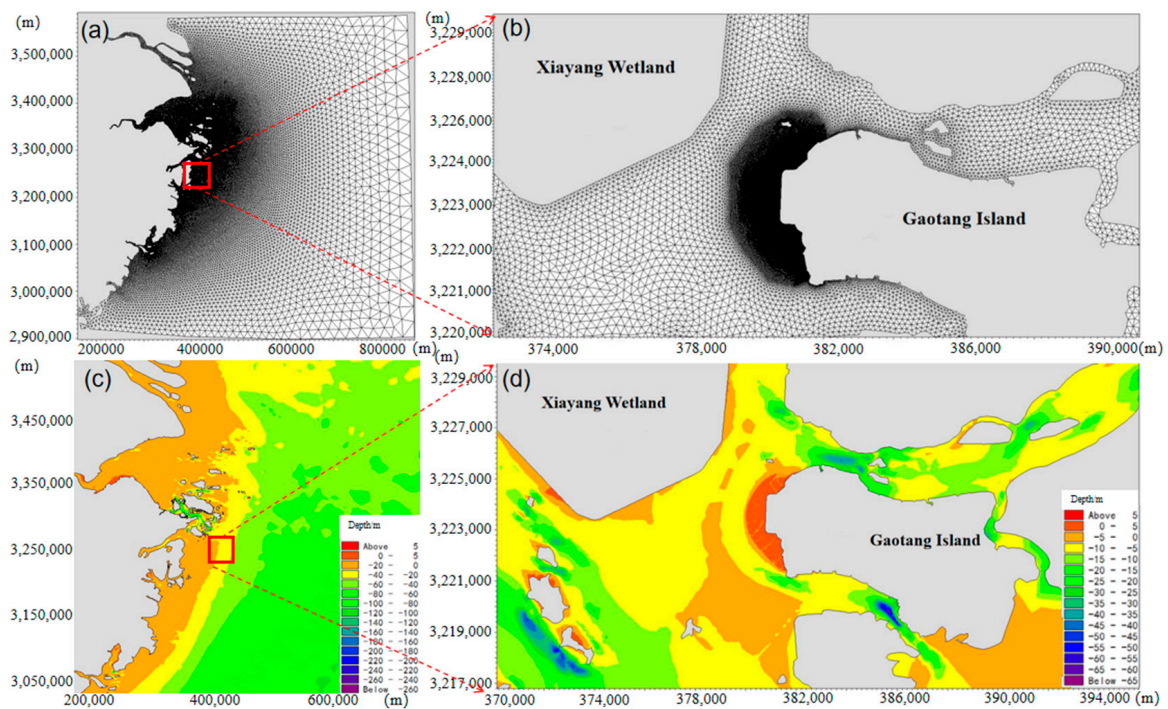


**Figure 6.** Model setup ((a). Schematic of the model calculation area; (b). Grid layout near the PV area; (c). Schematic of the large-scale bathymetric topography; (d). Schematic of the bathymetric topography in the PV area).

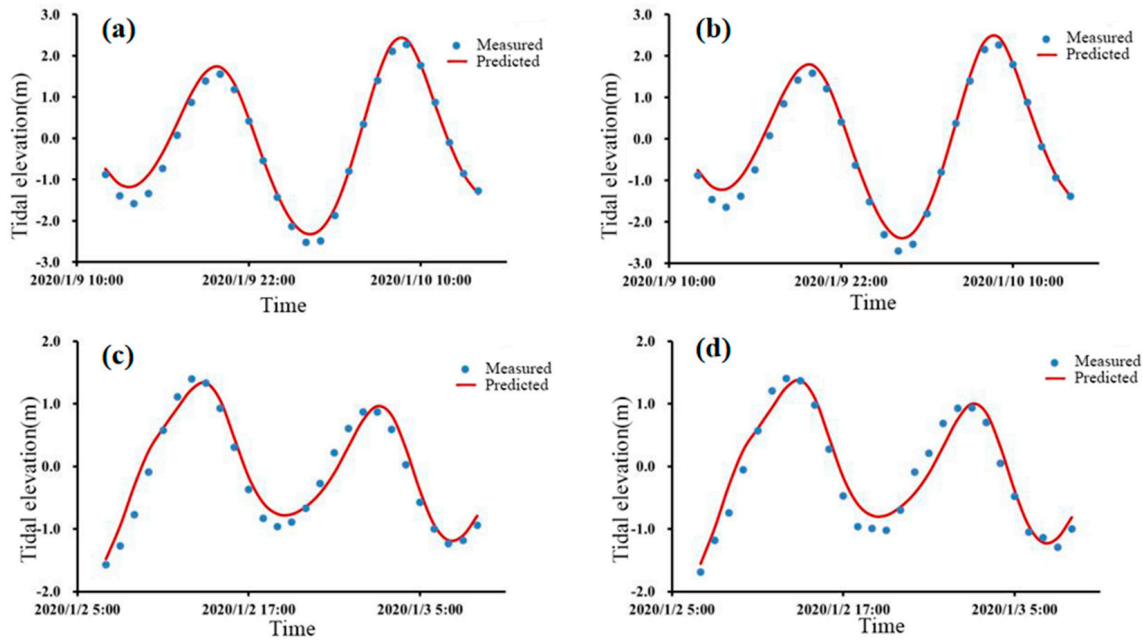


**Figure 7.** Tide level verification maps ((a). During high tide at station W1; (b). Tide level verification maps during high tide at station W2; (c). During low tide at station W1; (d). During low tide at station W2).

**Table 3.** Statistics on tide level errors.

Station Number	Tide	Tide Level Errors	
		(m)	(%)
W1	high	0.12	2.4
	low	0.16	5.5
W2	high	0.11	2.2
	low	0.18	6.4

For tidal flow verification, the flow velocity and direction data from six tidal flow stations in 2020 were used for verification, with the high tide period from 9 January 2020, 12:00 to 10 January 2020, 14:00 and the low tide period from 2 January 2020, 7:00 to 3 January 2020, 9:00. The results of each station’s flow velocity and direction are shown in Figure 8, and the specific flow velocity and direction errors are shown in Table 4. Overall, the simulation results for flow direction and velocity at each station are satisfactory, accurately reflecting the tidal flow characteristics in the PV area and meeting the requirements of the specifications. The model can be applied to various tasks such as forecasting after the construction of marine PV projects.

The impact of PV offshore facilities on the seabed topography comprises two parts: pile foundations and wave barriers. When modeling, the breakwater’s geometry is considered by modifying the closed boundary. Pile foundations are separated 5 m apart with a diameter of 600 mm. Their geometry isn’t considered into the modeling framework due to the large number and small size of pile foundations in this project.

The impact of pile foundations is generalized, and the additional resistance method is used to simulate the pile foundation effect. The specific formula is as follows [26]:

$$F = \frac{1}{2} \rho_w \gamma C_D A_e V^2 \tag{11}$$

where  $\rho_w$  is the density of water,  $\gamma$  is the kinematic viscosity coefficient of water,  $C_D$  is the drag coefficient,  $A_e$  is the projected area of the pile perpendicular to the water flow, and  $V$  is the flow rate acting on the pile.

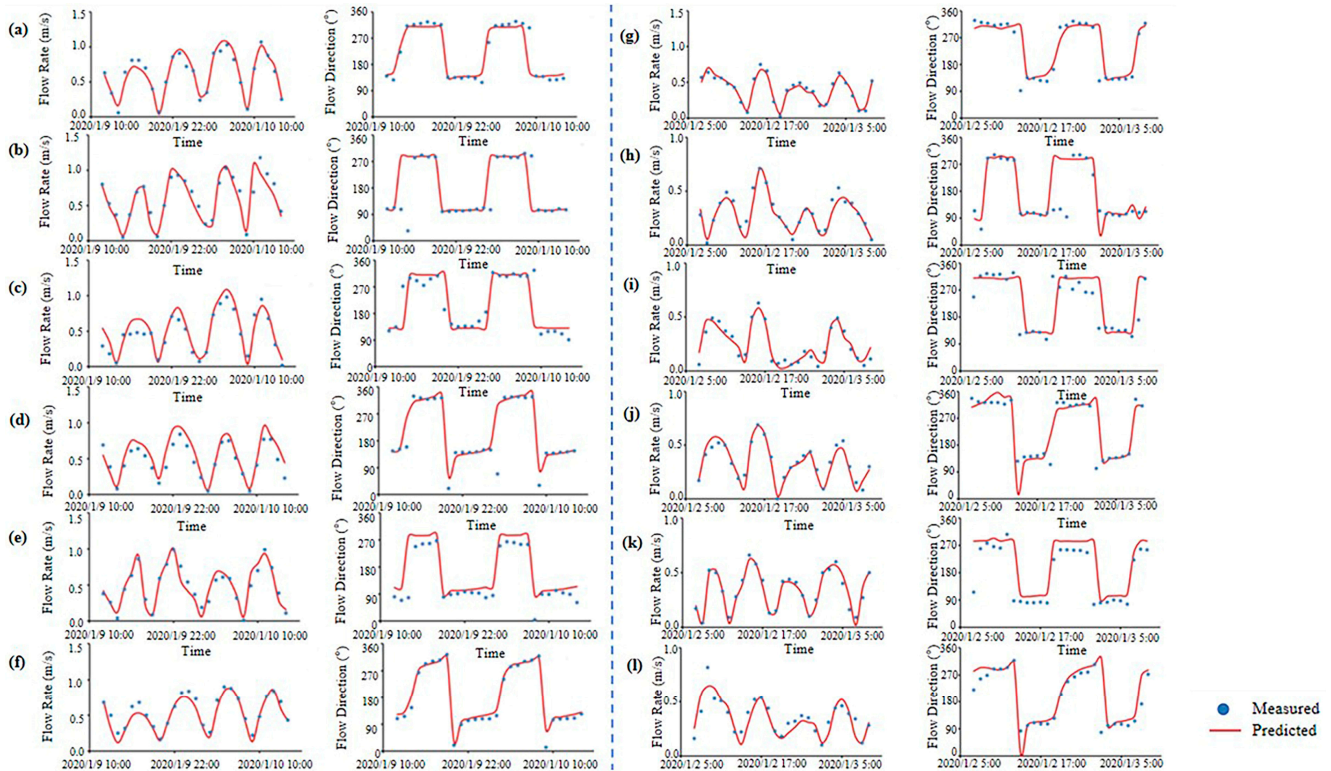


**Figure 8.** Flow velocity and flow direction validation ((a–f) for sites 1#–6#, high tide; (g–l) for sites 1#–6#, low tide).

**Table 4.** Statistics on flow velocity and flow direction errors.

Station Number	Average Flow Rate Error		Average Flow Direction Error	
	(m/s)	(%)	(°)	(%)
1	0.04	8.9	15	4.2
2	0.06	12.6	16	4.4
3	0.07	15.6	18	5.0
4	0.07	15.2	14	3.9
5	0.05	10.8	19	5.3
6	0.06	14.6	12	3.3

In DHI MIKE21FM, a database of pile foundation parameters has been embedded. As long as the parameters of pile foundation type, length and width scale, north angle, and elevation are input into the software (Version 2014), the software will automatically calculate the influence of the resistance of the pier.

#### 4.1.2. Analysis of the Tidal Field in the Marine PV Area

The simulation results for flow velocity at each station are good and generally reflect the actual characteristics of the flow field in the engineering area. To further understand the overall flow field distribution near the PV area, large-scale rising and falling rapids vector plots were obtained.

The flood and ebb flow fields near Sanmen Bay area are shown in Figure 9a,b. During flood tides, the main inflow is from the southeast of the offshore area into Sanmen Bay. After entering Sanmen Bay, the flow is divided into multiple branches flowing toward the bay’s head due to the numerous channels and waterways in the bay. The ebb flow routes and directions are generally opposite to the flood flow. The water flows from the bay’s head into Sanmen Bay and then flows into the East China Sea. The flood and ebb flow fields in the PV area are shown in Figure 9c,d. During flood tides, the flow converges from the

Sanmen Bay entrance with the flow between Gaotang Island and Hua'ao Island into the PV area on Gaotang Island. Due to the shallow nature of the PV area, the flow is weak. After passing through the PV area, the flow continues northward into Baijiao Waterway. During ebb tides, the ebb flow from Baijiao Waterway is divided into two branches, including one entering Shipu Waterway and the other flowing through the PV area. During ebb tides, extensive exposed areas occur in the PV area. Overall, the flood and ebb flow vectors in the PV area are generally regular, with obvious alternating flow characteristics.

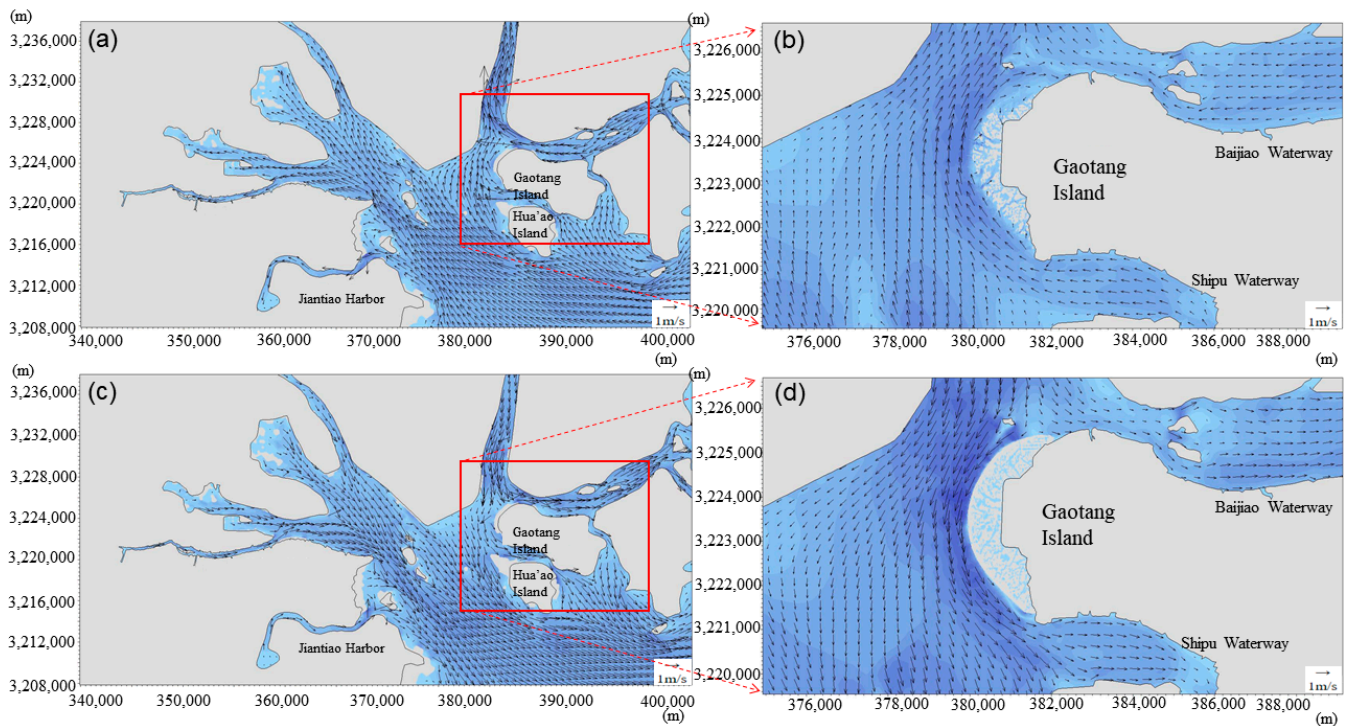


**Figure 9.** Rising and falling rapids field ((a). Vector map of large-scale rising rapids in Sanmen Bay; (b). Vector map of large-scale falling rapids in Sanmen Bay; (c). Map of rising rapids field in the study area; (d). Map of falling rapids field in the study area).

#### 4.1.3. Changes in Flow Vectors after the Completion of the PV Area

The offshore PV piles in the study area are set up as permeable structures, and do not change the overall shoreline in the study area. The study area is a shallow water area with high relief and weak tidal currents. Looking at the wide-range flow field before and after the project (Figure 10), it can be seen that there is little to no change in the direction of the ebb and flow currents in the wide-range sea area after the project, and they mainly maintain their original directions. Especially during the ebb tide, the installation of ocean PV systems has little impact on the current direction since the project area is mostly exposed. The flood tide current only undergoes slight changes in the shallow zone area, and there is no fundamental change in the wide-range flow direction.

#### 4.1.4. Prediction of Flow Velocity Changes in PV Zones

As shown in Figure 10, due to the obstruction of the wave barrier wall, the flow velocity is reduced at high tide, with a reduction range of 0.05~0.09 m/s. The influence range mainly focuses on the marine PV area surrounded by the wave barrier wall. At low tide, the range of flow velocity changes is much smaller than that during high tide, and due to the lower tide level, the outcropping of beaches occurs. Therefore, the flow velocity change mainly focuses on the wave barrier wall, and the flow velocity reduction ranges from 0.03 to 0.05 m/s. Overall, due to the influence of the wave barrier wall and PV pile foundation, the average flow velocity is reduced by 0.03~0.07 m/s. The current velocity in the marine PV area is mainly reduced due to the influence of the wave barrier wall and PV

piling, with the average current velocity reduced by 0.03~0.07 m/s (Figure 11). Overall, the change of current velocity is mainly concentrated in the area surrounded by the wave barrier wall and PV piling, with less influence on the surrounding channel and the wide range of the current field.

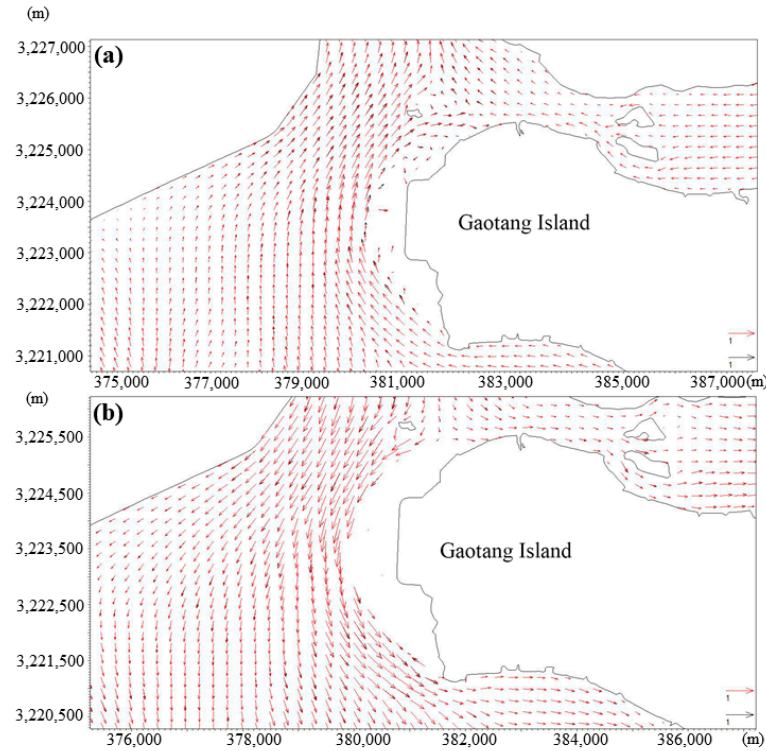


Figure 10. Comparison of flow vectors of high tide (a) and low tide (b) before and after the project (black is before the project, red is after the project).

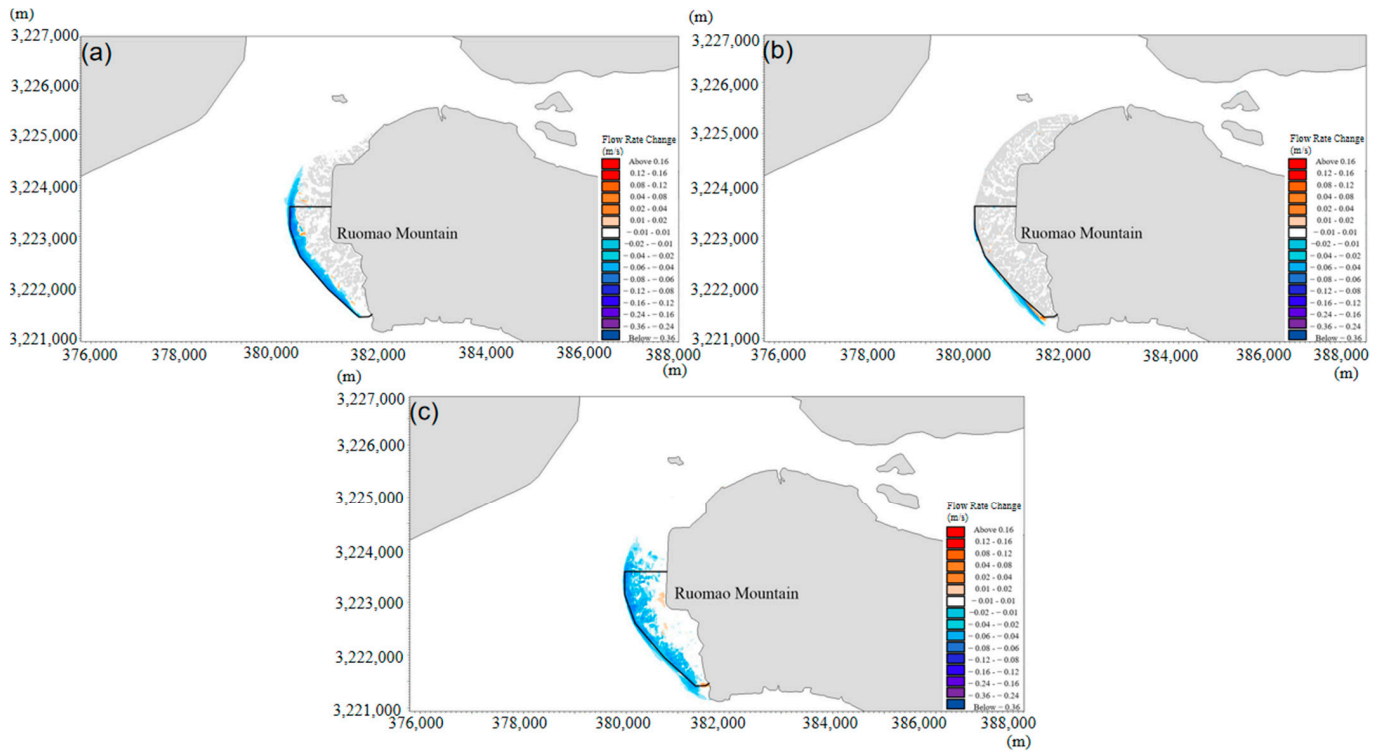
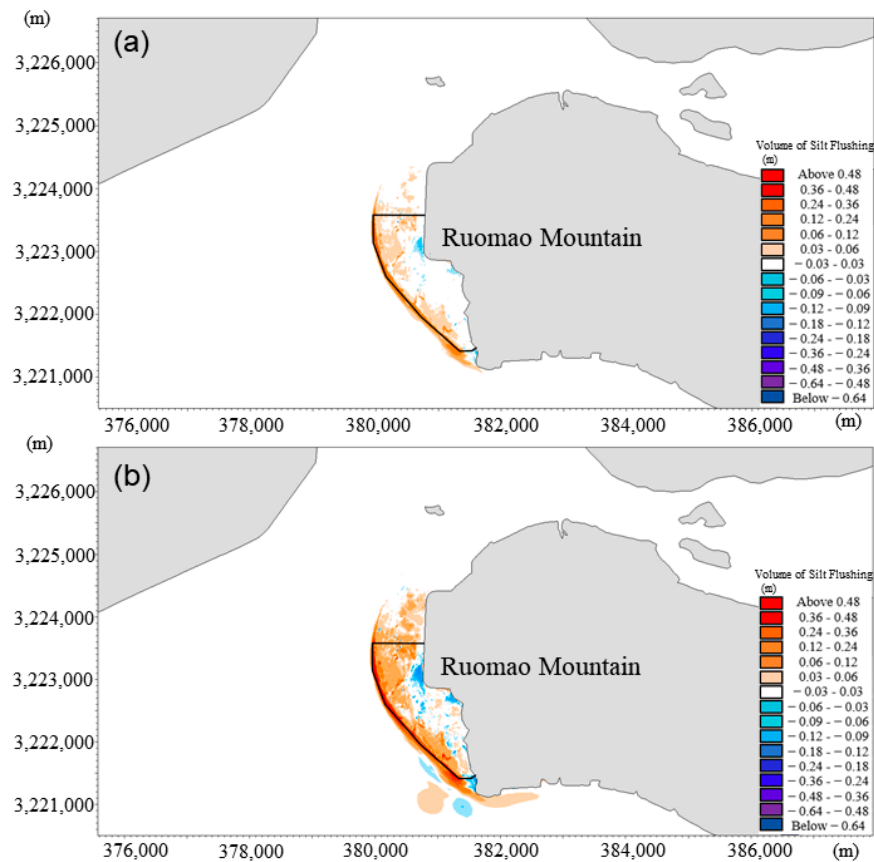


Figure 11. Distribution of flow velocity changes ((a). Post-engineering surge moments; (b). Post-engineering fall moments; (c). Post-engineering whole-tide mean flow velocity changes).

#### 4.1.5. Analysis of Environmental Impacts of Silt Flushing

In this paper, the effect of construction time was not considered, and only two simulations of the study area were performed before and after construction. The first year and final flushing siltation changes after the construction of marine PV are shown in Figure 12. From the siltation change, the area under the influence of marine PV is mainly concentrated in the sea area surrounded by the wave barrier wall and PV pile foundation, which is basically consistent with the trend of the current velocity change. In the first year of marine PV construction, siltation was mainly generated around the wave barrier wall project, and the thickness of siltation was between 0.12 and 0.20 m/a. The area where the PV pile foundation is located is an open beach most of the time due to the high terrain, so the siltation caused is not significant, with the annual siltation between 0.03~0.06 m/a, comprising slight scouring in some areas. When the siltation reaches equilibrium, the tide is weak due to most of the elevation in the marine PV area being above the mean low tide level. When the tidal current is weak, the water depth has a greater influence on the siltation intensity after reaching equilibrium with the siltation in the vicinity of the wave retaining wall, the south side of the marine photovoltaic area, and other depths with tidal current conditions, such as the areas of siltation with relatively larger grain sizes, where the final siltation being 0.4–0.6 m, and in most of the shallow areas, where the siltation thickness of the smaller grain sizes is the 0.06~0.09 m. There is a slight scouring in the sea area outside the marine PV area, with a scouring amplitude of 0.04~0.05 m. Overall, the scouring and siltation caused by the marine PV construction is mainly concentrated along the southwestern project area on Gaotang Island, which has less impact on the surrounding sea area and the navigation channel.



**Figure 12.** Changes in siltation ((a). Change in final siltation after the project; (b). Change in siltation in the first year after the project).

#### 4.2. Analysis of Ecological and Resource Impacts of Sea Use

##### 4.2.1. Ecological Impacts during Construction and Operation Periods

The construction of marine PV projects, such as pile foundation construction and the construction and removal of cofferdams, can cause disturbance to the sediments on the seabed in the local area, resulting in resuspension of the relatively stable sediments and forming high concentration-suspended sediment plumes [15]. Furthermore, sediments on the construction piers and submerged platforms can enter the sea area with rainfall. These pollution processes can cause turbidity in the local water area, reducing the transmittance of sunlight, affecting the migration of swimming organisms in the area, and causing varying degrees of impact on zooplankton [27]. Moreover, the decreased water transparency and reduced dissolved oxygen hinder the cell division and growth of phytoplankton, reducing the quantity of phytoplankton in the unit water volume and leading to a decrease in the primary productivity in the water area [28].

In addition, the high concentrations of suspended matter can affect the respiration, feeding, digestion, and reproduction of zooplankton [29]. Under the influence of high-concentration suspended matter, the feeding efficiency of filter-feeding and omnivorous species is decreased due to the adhesion of fine particles. The filtering efficiency of certain species that feed on other zooplankton decreases due to the various adverse effects of suspended matter, potentially leading to starvation due to a shortage of food. Predatory and omnivorous species may also experience a decrease in the density of prey organisms that they can feed on, resulting in hunger caused by food shortages. The density of other zooplankton that can be preyed upon by these species may also be reduced due to the adverse effects of excessive suspended matter.

##### 4.2.2. Analysis of Impacts on Marine Ecosystem Service Functions

The impact of offshore PV farm project construction on marine ecology and fisheries is ultimately reflected in the damage or loss of some ecosystem service functions [30]. Marine ecosystem service [31] function refers to the ecosystem and ecological processes formed and maintained by natural environmental conditions and utility for human survival. The ecosystem service function of the sea can be divided into three dominant functions including species habitat, aquaculture production, and pollution purification.

- Species habitat:

The construction period of the PV farm project will cause some disturbance to the aquatic animals in the region in terms of habitat and foraging, mainly causing a certain degree of harm to the juveniles but avoiding injury to the adults.

- Aquaculture production:

Marine ecosystems synthesize and produce organic matter and its products that are necessary for human survival through primary and secondary production [32,33]. Marine PV power generation projects can be carried out under the PV panels for mudflat aquaculture, which have little impact on aquaculture production.

- Pollutant purification:

The ocean is a huge purifier, which has a certain comprehensive ability to dilute, diffuse, oxidize, reduce and degrade the pollutants entering the sea. The construction period of marine PV construction will increase the suspended sediment in the sea area and weaken photosynthesis, which will have a certain impact on the pollutant purification function, but the impact time will be short-lived. During the operation period, it is not expected to change the characteristics of the tidal field of the sea area. At the same time, it will not change the pollutant load of the sea area and will not produce suspended sediments, so it will not cause obvious changes to the pollutant purification function of the sea area.

### 4.2.3. Loss of Marine Life

#### (1) Intertidal organisms

The project uses  $\phi 300$  mm PHC piles, about 100,000 piles, for PV mounts, box transformers (inverter-booster integrated machine), and cable mounts. A total of 1600 piles, 600 mm PHC piles, are used in the wave blocking facilities. The total area of sea directly occupied by the piles is  $0.75 \text{ hm}^2$ , all of which are intertidal mudflats, and this part of intertidal zone will be occupied permanently. The temporary sea area for construction cofferdam is  $3.8 \text{ km} \times 6 \text{ m} = 2.28 \text{ hm}^2$ . The construction of the cofferdam is a temporary project, and all intertidal organisms in the cofferdam area will be lost during the period of use and can be gradually restored after removing the cofferdam.

Within the cofferdam area, except for the pile foundation area with a compensation of 20 years, the rest of the area also suffered a one-time disturbance of sorts and need to include 3 years for compensation calculation. The area of this part is  $162.0836 - 0.75 = 161.3336 \text{ hm}^2$ .

Intertidal biological loss calculation: the project occupied sea area is located within the intertidal zone, and the piling occupied intertidal zone organisms will be likely be permanently lost but can be gradually recovered after removing the temporary cofferdam, and the disturbed area can be recovered after the end of the construction of the temporary cofferdam enclosure (Table 5). During the March 2017 survey, the biomass of the intertidal zone around the project's T5 was  $27.56 \text{ g/m}^2$ , and the biomass of the intertidal zone around the project's T6 was  $21.3 \text{ g/m}^2$  during the September 2020 survey. The average biomass for both seasons was  $24.43 \text{ g/m}^2$ .

**Table 5.** Summary of biotic losses in the intertidal zone.

Project Components	Occupied Intertidal Area (ha)	Intertidal Biomass ( $\text{g/m}^2$ )	One-Time Loss of Biomass (t)	Compensation Years	Loss of Biomass (t)
Permanent sea occupation	0.75	24.43	0.18	20	3.6
Cofferdam occupied sea area	2.28		0.56	3	1.68
Disturbed area within the cofferdam	161.3336		39.39	3	118.17
Total			40.13		123.45

#### (2) Impacts of suspended sediment dispersion on zooplankton and fishery resources

The construction of marine PV systems is expected to increase the concentration of suspended solids in local seawater, reduce light transmittance, hinder the photosynthesis of phytoplankton, reduce the quantity of phytoplankton per unit of water, ultimately leading to a decline in the primary productivity levels in nearby waters. The reduction in light transmittance may disrupt the living habits of certain zooplankton, which rely on variations in light intensity for vertical migration, or cause feeding difficulties for some organisms. Suspended solids can also stimulate marine organisms, making it challenging for them to inhabit and escape the vicinity, thus reducing the diversity and quantity of swimming animals in nearby waters [34].

Since the suspended sediment from pile foundation construction is located within the temporary cofferdam, it will not cause any change in the concentration of suspended sediment in the surrounding sea area. This study only calculates the impact of suspended sediment caused by the construction and removal of the cofferdam on the surrounding marine organisms. The ecological data are quoted as the average of the March 2017 survey data and the September 2020 survey data. Data on the loss of living marine resources and compensation due to the spreading of suspended sediments from cofferdam construction and removal are shown in Tables 6 and 7.

**Table 6.** List of marine living resources lost and compensated for, as a result of spreading of suspended sediments from cofferdam construction.

Fisheries Resources	Concent-Ration	Diffusion Area (m <sup>2</sup> )	Average Water Depth (m)	Diffusion Volume (m <sup>3</sup> )	Resource Density	Loss Rate	Survival Rate	One-time Loss Volume	Duration of Impact	Continuing Loss Volume
Phytoplank-ton	10~100 mg/L	1,870,000	1.3	2,431,000	$1.7 \times 10^5$ ind/m <sup>3</sup>	20%	/	$826.54 \times 10^8$	1	$13.59 \times 10^{10}$ cells
	100~150 mg/L	270,000	1.3	351,000		30%		$179.01 \times 10^8$		
	>150 mg/L	320,000	1.3	416,000		50%		$353.6 \times 10^8$		
Zooplankt-on	10~100 mg/L	1,870,000	1.3	2,431,000	66.9 mg/m <sup>3</sup>	20%	10% converted to lower swimming animals	3252.678 g	1	5.35 kg
	100~150 mg/L	270,000	1.3	351,000		30%		704.457 g		
	>150 mg/L	320,000	1.3	416,000		50%		1391.52 g		
Fish eggs	10~100 mg/L	1,870,000	1.3	2,431,000	0.16 grains/m <sup>3</sup>	20%	1%	777.92 grains	1	$1.28 \times 10^3$ grains
	100~150 mg/L	270,000	1.3	351,000		30%		168.48 grains		
	>150 mg/L	320,000	1.3	416,000		50%		332.8 grains		
Juvenile fish	10~100 mg/L	1,870,000	1.3	2,431,000	0.248 tails/m <sup>3</sup>	20%	5%	6028.88 tails	1	$9.91 \times 10^3$ tails
	100~150 mg/L	270,000	1.3	351,000		30%		1305.72 tails		
	>150 mg/L	320,000	1.3	416,000		50%		2579.2 tails		
Adult fish	10~100 mg/L	1,870,000	/	/	0.249 g/m <sup>2</sup>	10%	/	46,563 g	1	75.94 kg
	100~150 mg/L	270,000	/	/		20%		13,446 g		
	>150 mg/L	320,000	/	/		20%		15,936 g		

Note: Losses due to the spread of suspended sediment from weir construction were as follows: phytoplankton,  $13.59 \times 10^{10}$  cells; zooplankton density, 5.35 kg; fish eggs,  $1.28 \times 10^3$ ; juvenile fish,  $9.91 \times 10^3$ ; and adult fish, 75.94 kg.

**Table 7.** List of marine living resources lost, as a result of the removal of cofferdams and dispersal of suspended sediments and their compensation.

Fisheries Resources	Concent-Ration	Diffusion Area (m <sup>2</sup> )	Average Water Depth (m)	Diffusion Volume (m <sup>3</sup> )	Resource Density	Loss Rate	Survival Rate	One-Time Loss Volume	Duration of Impact	Continuing Loss Volume
Phytopla-nkton	10~100 mg/L	1,150,000	1.3	1,495,000	$1.7 \times 10^5$ ind/m <sup>3</sup>	20%	/	$508.3 \times 10^8$	1	$6.30 \times 10^{10}$ cells
	100~150 mg/L	50,000	1.3	65,000		30%		$33.15 \times 10^8$		
	>150 mg/L	80,000	1.3	104,000		50%		$88.4 \times 10^8$		
Zooplank-ton	10~100 mg/L	1,150,000	1.3	1,495,000	66.9 mg/m <sup>3</sup>	20%	10% converted to lower swimming animals	2000.31 g	1	2.48 kg
	100~150 mg/L	50,000	1.3	65,000		30%		130.455 g		
	>150 mg/L	80,000	1.3	104,000		50%		347.88 g		
Fish eggs	10~100 mg/L	1,150,000	1.3	1,495,000	0.16 grains/m <sup>3</sup>	20%	1%	478.4 grains	1	$0.59 \times 10^3$ grains
	100~150 mg/L	50,000	1.3	65,000		30%		31.2 grains		
	>150 mg/L	80,000	1.3	104,000		50%		83.2 grains		
Juvenile fish	10~100 mg/L	1,150,000	1.3	1,495,000	0.248 tails/m <sup>3</sup>	20%	5%	3707.6 tails	1	$4.59 \times 10^3$ tails
	100~150 mg/L	50,000	1.3	65,000		30%		241.8 tails		
	>150 mg/L	80,000	1.3	104,000		50%		644.8 tails		
Adult fish	10~100 mg/L	1,150,000	/	/	0.249 g/m <sup>2</sup>	10%	/	28,635 g	1	35.11 kg
	100~150 mg/L	50,000	/	/		20%		2490 g		
	>150 mg/L	80,000	/	/		20%		3984 g		

Note: Losses due to diffusion of suspended sediment from cofferdam removal were as follows: phytoplankton,  $6.30 \times 10^{10}$  cells; zooplankton density, 2.48 kg; fish eggs,  $0.59 \times 10^3$ ; juvenile fish,  $4.59 \times 10^3$ ; and adult fish, 35.11 kg.

## 5. Discussion and Outlook

### 5.1. Marine PV Construction Planning

The advantages of marine PV power stations lie in improving water quality [35,36], reducing water evaporation [37,38], increasing the efficiency of PV power generation systems, not subject to available terrestrial land resources, and in facilitating convenient construction and maintenance [26]. Marine PV construction falls under the category of industrial use of the sea. It should be compatible with industrial use, urban construction, and tourism and entertainment requirements, without affecting basic functions such as port shipping. Marine PV power projects falls into the category of marine new energy industry and should provide clean electricity for surrounding industries and urban construction, ensuring no new land reclamation and no pollution emissions from power generation, reducing the pressure on terrestrial thermal power generation and moderately controlling emissions from land-based pollutants to improve marine water quality.

### 5.2. Site Selection Rationality

Site selection for marine PV construction [39–41] should strive to: (1) Choose economically developed areas with high electricity demand. The construction of PV power stations should follow the principle of building projects near regions with high electricity loads, especially in the central and eastern cities, and industrial areas where industrial and commercial foundations are strong; (2) Seek favorable regional construction and operating conditions by selecting regions with convenient water transportation, well-equipped water, power, good communication facilities, while at the same time ensuring that the chosen sea area has suitable water depth and marine conditions to support the installation and operation of PV equipment. Conditions such as waves and tidal currents in the water should also be assessed; (3) Ensure high regional policy support. As marine civilization construction advances, and the development and utilization of clean electricity are advocated at the national level, regional governments should formulate corresponding policies to actively promote the green development of the marine economy; (4) Select a compatible balance between natural resources utilization and ecological environmental conservation. Choose regions with good sunlight conditions to ensure that PV cells can fully absorb solar energy. Consider the potential impact of site selection on the marine ecosystem. Ensure that measures are taken during site selection and construction to minimize negative impacts on the marine ecological environment; (5) Link coordination with surrounding marine activities. Through reasonable construction and protective measures, minimize the impact of marine PV construction on the stability of seawater.

### 5.3. Measures for Marine Area Use

Essentially, any development and utilization of the ocean must first seek to protect marine resources, with economic development adopting a path that strengthens environmental protection. To maintain marine health, protect the marine ecological environment, and ensure the sustainable development of marine resources and the marine economy, it is essential to strengthen comprehensive marine management. Rational development of marine resources, the construction of a well-functioning marine ecosystem, and coordination with the sustainable development of the marine economy should always be emphasized. In addition, marine units should effectively implement coordination agreements or schemes with stakeholders to ensure marine order and jointly uphold the harmonious development of the marine environment [42]. Marine functional zoning is a scientific basis for marine area management and is a crucial way to achieve the rational development and sustainable utilization of marine areas. In managing marine functional zoning, attention should be paid to the compatibility and exclusivity of functional zones, the maintenance of the natural attributes and quality of functional zones, and the connection and protection of adjacent functional zones. Construction projects should focus on the integrity of the functional zone system and the main functions of key marine areas. Zoning should comply with water quality and sediment quality standards, while protecting the industrial layout of adjacent

marine areas. There should be strict adherence to marine functional zoning as the basis for marine ecological environmental protection. If other resources near the construction areas of marine PVs need to be developed and utilized, it should be based on marine functional zoning and strict ecological protection measures should be taken to prevent damage to coastal beaches, vegetation, and marine ecological environments [43].

## 6. Conclusions

This study aimed to investigate the marine hydrodynamics in the offshore PV area situated in the northern part of the long growth coast at the west beach of Gaotang Island, Xiangshan County, Ningbo City, Zhejiang Province. This study utilized measured marine hydrographic data in conjunction with the MIKE21FM model. The simulation results accurately reflect the tidal characteristics in the PV sea area, meeting regulatory requirements. There is a clear regularity in the overall ebb and flow of tides in the PV sea area. The construction of marine PVs has little impact on the tidal vector, with only slight changes in upwelling tidal currents in shallow areas. There is no fundamental change in the large-scale tidal vector. The variation in flow velocity in the marine PV area is mainly concentrated in the area surrounded by wave barriers and PV piles. The impact on surrounding channels and large-scale flow fields is relatively small. The erosion and sedimentation caused by marine PV projects have minimal effects on the surrounding sea areas and channels. The construction of marine PVs will have a certain degree of impact on the ecology and resources of the surrounding sea areas. It will result in losses of marine organisms. Therefore, in the planning and construction of marine PVs, it is necessary to comprehensively consider factors such as policies, economics, and the environment. These will allow for better planning and construction of marine photovoltaic projects for sustainable economic, environmental, and social development. Overall, offshore PV projects have unique technical and regulatory requirements. They effectively utilize offshore space to provide clean power resources to nearby areas.

**Author Contributions:** Writing—original draft preparation, P.W., J.Z. and F.Z.; methodology and software, X.J., X.L. (Xingwen Lin) and K.Z.; conceptualization and funding acquisition, P.W. and F.Z.; writing—review and editing, J.S., N.W.C. and M.L.T.; data curation, X.L. (Xia Lin) and X.M.; validation and visualization, K.Z. and J.W. All authors have read and agreed to the published version of the manuscript.

**Funding:** This research was carried out with the Monitoring and evaluation of ocean space resource in six major bay areas of Zhejiang Province, Department of Natural Resources of Zhejiang Province (No. 330000200100313013010).

**Institutional Review Board Statement:** Not applicable.

**Informed Consent Statement:** Not applicable.

**Data Availability Statement:** Some or all of the data that support the findings of this study are available from the corresponding author upon reasonable request.

**Acknowledgments:** We appreciate the anonymous reviewers and editors for appraising our manuscript and for offering constructive comments.

**Conflicts of Interest:** Author Xinfei Jin was employed by the company Shengyong Marine Technology Limited Company of Ningbo. The remaining authors declare that the research was conducted in the absence of any commercial or financial relationships that could be construed as a potential conflict of interest.

## References

1. Wilberforce, T.; Baroutaji, A.; El Hassan, Z.; Thompson, J.; Soudan, B.; Olabi, A.G. Prospects and challenges of concentrated solar photovoltaics and enhanced geothermal energy technologies. *Sci. Total Environ.* **2019**, *659*, 851–861. [[CrossRef](#)] [[PubMed](#)]
2. Jiang, J.X.; Gao, X.Q. Research progress on climate effect and influence mechanism of photovoltaic systems. *Plateau Meteorol.* **2022**, *41*, 953–962. (In Chinese) [[CrossRef](#)]

3. Dunnett, S.; Sorichetta, A.; Taylor, G. Harmonised global datasets of wind and solar farm locations and power. *Sci. Data* **2020**, *7*, 130. [[CrossRef](#)] [[PubMed](#)]
4. Breyer, C.; Bogdanov, D.; Gulagi, A.; Aghahosseini, A.; Barbosa, L.S.N.S.; Koskinen, O.; Barasa, M.; Caldera, U.; Afanasyeva, S.; Chile, M.; et al. On the role of solar photovoltaics in global energy transition scenarios. *Prog. Photovolt.* **2017**, *25*, 727–745. [[CrossRef](#)]
5. Schuman, S.; Lin, A. China's Renewable Energy Law and its impact on renewable power in China: Progress, challenges and recommendations for improving implementation. *Energy Policy* **2013**, *51*, 89–109. [[CrossRef](#)]
6. Mercado, L.M.; Bellouin, N.; Sitch, S.; Boucher, O.; Huntingford, C.; Wild, M.; Cox, P.M. Impact of changes in diffuse radiation on the global land carbon sink. *Nature* **2009**, *458*, 1014–1017. [[CrossRef](#)] [[PubMed](#)]
7. Araki, K.; Nagai, H.; Lee, K.H.; Yamaguchi, M. Analysis of impact to optical environment of the land by flat-plate and array of tracking PV panels. *Sol. Energy* **2017**, *144*, 278–285. [[CrossRef](#)]
8. Armstrong, A.; Ostle, N.J.; Whitaker, J. Solar park microclimate and vegetation management effects on grassland carbon cycling. *Environ. Res. Lett.* **2016**, *11*, 074016. [[CrossRef](#)]
9. Zhou, L.M.; Tian, Y.H.; Roy, S.B.; Thorncroft, C.; Bosart, L.F.; Hu, Y.L. Impacts of wind farms on land surface temperature. *Nat. Clim. Chang.* **2012**, *2*, 539–543. [[CrossRef](#)]
10. Liu, L.Q.; Wang, Z.X.; Zhang, H.Q.; Xue, Y.C. Solar energy development in China-A review. *Renew. Sustain. Energy Rev.* **2010**, *14*, 301–311. [[CrossRef](#)]
11. Li, P.D.; Gao, X.Q.; Jiang, J.X.; Yang, L.W.; Li, Y.J. Characteristic Analysis of Water Quality Variation and Fish Impact Study of Fish-Lighting Complementary Photovoltaic Power Station. *Energies* **2020**, *13*, 4822. [[CrossRef](#)]
12. Gao, J.W.; Guo, F.J.; Li, X.Z.; Huang, X.; Men, H.J. Risk assessment of offshore photovoltaic projects under probabilistic linguistic environment. *Renew. Energy* **2021**, *163*, 172–187. [[CrossRef](#)]
13. Trapani, K.; Millar, D.L. Proposing offshore photovoltaic (PV) technology to the energy mix of the Maltese islands. *Energy Convers. Manag.* **2013**, *67*, 18–26. [[CrossRef](#)]
14. Wu, S.; Jiang, N.; Zhang, S.; Zhang, P.P.; Zhao, P.; Liu, Y.; Wang, Y.H. Discussion on the development of offshore floating photovoltaic plants, emphasizing marine environmental protection. *Front. Mar. Sci.* **2024**, *11*, 1336783. [[CrossRef](#)]
15. Ghosh, A. A comprehensive review of water based PV: Flotovoltaics, under water, offshore & canal top. *Ocean Eng.* **2023**, *281*, 115044. [[CrossRef](#)]
16. Sun, Y.W.; Li, Y.; Wang, R.; Ma, R.F. Assessing the national synergy potential of onshore and offshore renewable energy from the perspective of resources dynamic and complementarity. *Energy* **2023**, *279*, 128106. [[CrossRef](#)]
17. Ma, X.D.; Yu, H.M.; Zhang, D.Z.; Li, G.; Wan, J.Y.; Cai, D.Q. Analysis of the development trend of the water surface PV industry. *Sol. Energy* **2023**, *8*, 5–12. (In Chinese) [[CrossRef](#)]
18. GB12763-2007; Specifications for Oceanographic Survey. Standardization Administration: Beijing, China, 2007.
19. GB17378.7-2007; The Specification for Marine Monitoring. Standardization Administration: Beijing, China, 2007.
20. SC/9403-2012; Technical Specification for Marine Fishery Resources Sources. Ministry of Agriculture and Rural Affairs of the People's Republic of China: Beijing, China, 2013.
21. SC/T9110-2007; Technical Regulations for Impact Assessment of Construction Projects on Marine Living Resources. Ministry of Agriculture and Rural Affairs of the People's Republic of China: Beijing, China, 2008.
22. Zhu, C.J.; Liang, Q.; Yan, F.; Hao, W.L. Reduction of Waste Water in Erhai Lake Based on MIKE21 Hydrodynamic and Water Quality Model. *Sci. World J.* **2013**, *2013*, 958506. [[CrossRef](#)]
23. SC/T 9110-2007; Technical Procedures for Evaluating the Impact of Construction Projects on Marine Living Resources. Chinese Academy of Fishery Sciences: Beijing, China, 2007.
24. GB 11607; Water Quality Standard for Fisheries. Ministry of Ecology and Environment of the People's Republic of China: Beijing, China, 1989.
25. GB 3097; Sea Water Quality Standard. Ministry of Ecology and Environment of the People's Republic of China: Beijing, China, 2003.
26. Ren, Z.J.; Wang, Z.A.; Lu, H.J. Mike21 Application of Software Pile Group Generalization Methods to High-Pile Wharves. *Port Waterw. Eng.* **2017**, *10*, 118–124. [[CrossRef](#)]
27. Hooper, T.; Armstrong, A.; Vlaswinkel, B.; Centre, L.E.; La, L. Environmental impacts and benefits of marine floating solar. *Sol. Energy* **2021**, *219*, 11–14. [[CrossRef](#)]
28. Taormina, B.; Bald, J.; Want, A.; Thouzeau, G.; Lejart, M.; Desroy, N.; Carlier, A. A review of potential impacts of submarine power cables on the marine environment: Knowledge gaps, recommendations and future directions. *Renew. Sustain. Energy Rev.* **2018**, *96*, 380–391. [[CrossRef](#)]
29. Ziar, H.; Prudon, B.; Lin, F.V.; Roeffen, B.; Heijkoop, D.; Stark, T.; Teurlincx, S.; Domis, L.S.; Goma, E.G.; Extebarria, J.G.; et al. Innovative floating bifacial photovoltaic solutions for inland water areas. *Prog. Photovolt. Res. Appl.* **2020**, *29*, 725–743. [[CrossRef](#)]
30. Zhang, N.; Duan, H.B.; Shan, Y.L.; Reed Miller, T.; Yang, J.K.; Bai, X.M. Booming solar energy is encroaching on cropland. *Nat. Geosci.* **2023**, *16*, 932. [[CrossRef](#)]
31. Shen, C.C.; Zheng, W.; Shi, H.H.; Ding, D.W.; Wang, Z.L. Assessment and regulation of ocean health based on ecosystem services: Case study in the Laizhou Bay, China. *Acta Oceanol. Sin.* **2015**, *34*, 61–66. [[CrossRef](#)]
32. Pringle, A.M.; Handler, R.M.; Pearce, J.M. Aquavoltaics: Synergies for dual use of water area for solar photovoltaic electricity generation and aquaculture. *Renew. Sustain. Energy Rev.* **2017**, *80*, 572–584. [[CrossRef](#)]

33. Imani, M.; Fakour, H.; Lo, S.L.; Yuan, M.H.; Chen, C.K.; Mobasser, S.; Muangthai, I. Aquavoltaics Feasibility Assessment: Synergies of Solar PV Power Generation and Aquaculture Production. *Water* **2023**, *15*, 987. [[CrossRef](#)]
34. Zhang, G.Y.; Gu, H.B.; Wang, W.Y.; Zhang, S.L.; Xue, L.F. Evaluation of Subdaily Hydrological Regime Alteration Characteristics for Hydro–Photovoltaic Complementary Operation in the Upper Yellow River. *Water* **2024**, *16*, 300. [[CrossRef](#)]
35. Song, F.W.; Lu, Z.Q.; Guo, Z.H.; Wang, Y.; Ma, L. The Effects of a Fishery Complementary Photovoltaic Power Plant on the Near-Surface Meteorology and Water Quality of Coastal Aquaculture Ponds. *Water* **2024**, *16*, 526. [[CrossRef](#)]
36. Martínez, G.G.; Martín, M.A.P. Water Management Adaptation to Climate Change in Mediterranean Semiarid Regions by Desalination and Photovoltaic Solar Energy, Spain. *Water* **2023**, *15*, 3239. [[CrossRef](#)]
37. Aschale, T.M.; Sciuto, G.; Peres, D.J.; Gullotta, A.; Cancelliere, A. Evaluation of Reference Evapotranspiration Estimation Methods for the Assessment of Hydrological Impacts of Photovoltaic Power Plants in Mediterranean Climates. *Water* **2022**, *14*, 2268. [[CrossRef](#)]
38. Tay, Z.Y. Three-Dimensional Hydroelasticity of Multi-Connected Modular Offshore Floating Solar Photovoltaic Farm. *J. Mar. Sci. Eng.* **2023**, *11*, 1968. [[CrossRef](#)]
39. Hasti, F.; Mamkhezri, J.; McFerrin, R.; Pezhooli, N. Optimal solar photovoltaic site selection using geographic information system–based modeling techniques and assessing environmental and economic impacts: The case of Kurdistan. *Sol. Energy* **2023**, *262*, 111807. [[CrossRef](#)]
40. Colak, H.; Tugba, M.; Yasin, G. Optimal site selection for solar photovoltaic (PV) power plants using GIS and AHP: A case study of Malatya Province, Turkey. *Renew. Energy* **2020**, *149*, 565–576. [[CrossRef](#)]
41. Zhang, Y.; Tian, Z.Q.; Liu, B.L.; Chen, S.Y.; Wu, J.H. Effects of photovoltaic power station construction on terrestrial ecosystems: A meta-analysis. *Conserv. Restor. Ecol.* **2023**, *11*, 1151182. [[CrossRef](#)]
42. Clive, S. Geographical Dimensions to Global Oceans Governance. *Geogr. Rev.* **2021**, *113*, 20–47. [[CrossRef](#)]
43. Malone, T.C.; DiGiacomo, P.M.; Gonçalves, E.; Knap, A.H.; Talaue-McManus, L.; de Mora, S.; Muelbert, J. Enhancing the Global Ocean Observing System to meet evidence based needs for the ecosystem-based management of coastal ecosystem services. *Nat. Resour. Forum* **2014**, *38*, 168–181. [[CrossRef](#)]

**Disclaimer/Publisher’s Note:** The statements, opinions and data contained in all publications are solely those of the individual author(s) and contributor(s) and not of MDPI and/or the editor(s). MDPI and/or the editor(s) disclaim responsibility for any injury to people or property resulting from any ideas, methods, instructions or products referred to in the content.